8 LH-wave

8.1 Dispersion relation

The dielectric tensor $\overleftrightarrow{\epsilon}$ can be very complex depending on the situation and the phenomena that are investigated. One can add a tremendous amount of physics in it e.g. relative effects, collisions, warm or hot plasma effects and anisotropy. In case of LH waves, the cold plasma approximation ($v_{ph} \gg v_{th}$) is enough to get a reasonable accuracy in the dispersion relation except near the resonance where hot plasma effects are important. The warm plasma effect on the dispersion relation is described in next section. Using this approximation of the dielectric tensor $\overleftrightarrow{\epsilon}$ and if the coordinates axes are chosen so that the magnetic field is along the z-axis and the wave propagates in the x-z plane, the wave equation can be expressed in a matrix form

$$\begin{pmatrix} S - N_{\parallel}^2 & iD & N_{\perp}N_{\parallel} \\ iD & S - N^2 & 0 \\ N_{\perp}N_{\parallel} & 0 & P - N_{\perp}^2 \end{pmatrix} \cdot \begin{pmatrix} E_x \\ E_y \\ E_z \end{pmatrix} = 0, \tag{2}$$

where,

$$S = 1 - \frac{\omega_{pe}^2}{\omega^2 - \omega_{ce}^2} - \frac{\omega_{pi}^2}{\omega^2 - \omega_{ci}^2} \tag{3}$$

$$iD = i\frac{\omega_{pi}^2\omega_{ci}}{\omega(\omega^2 - \omega_{ci}^2)} - i\frac{\omega_{pi}^2\omega_{ce}}{\omega(\omega^2 - \omega_{ce}^2)} \tag{4}$$

$$P = 1 - \frac{\omega_{pe}^2}{\omega^2} - \frac{\omega_{pi}^2}{\omega^2} \tag{5}$$

Where, ω_{pe} is electron plasma frequency, ω_{pi} is ion plasma frequency, ω_{ce} is electron cyclotron frequency, and ω_{ci} is ion cyclotron frequency. And, the notation $N_x \cong N_{\perp}$, $N_z \cong N_{\parallel}$ is adopted. The subscripts parallel and perpendicular refer to the direction of the external magnetic field $\mathbf{B_0}$. In order to have non trivial solutions the determinant of the multiplying matrix has to be zero. This condition gives the dispersion relation

$$D(N, \omega) = AN_{\perp}^4 + BN_{\perp}^2 + C = 0 \tag{6}$$

where,

$$A = S \tag{7}$$

$$B = (N_{\parallel}^2 - S)(S + P) + D^2 \tag{8}$$

$$C = P\left[(N_{\parallel}^2 - S)^2 - D^2\right]. \tag{9}$$

An approximation form of the dispersion relation, known as the ' electrostatic approximation,' is used frequently in lower-hybrid theories. The electrostatic approximation is given by,

$$SN_{\perp}^2 + PN_{\parallel}^2 = 0. \tag{10}$$

8.2 Wave propagation and accessibility

The perpendicular refractive index $N_\perp$ can be solved from Eq. (6)

$$N_\perp^2 = \frac{-B \pm \sqrt{B^2 - 4AC}}{2A}, \tag{11}$$

where the plus sign corresponds the slow wave and the minus sign is for the fast wave. In the case of LH grill the sign of the $N_\perp$ must be chosen so that the energy of the wave goes radially outward, and if imaginary, is damped.

There exits a wave resonance ($N_\perp \to \infty$) when the denominator of Eq. (11) goes to zero. Equating Eq. (3) to zero and solving it for the frequency gives, in the limit of $\omega_{ci} \ll \omega \ll \omega_{ce}$, the resonance frequency

$$\omega_{LH} = \omega_{pi} \left(1 + \frac{\omega_{pe}^2}{\omega_{ce}^2} \right)^{-1/2} \tag{12}$$

where, ω_{LH} is the lower hybrid resonance frequency. In the early days of LH heating the power was proposed to be absorbed by this resonance but later due to the accessibility conditions and strong Landau damping it was abandoned. Since then also other heating schemes e.g. stochastic ion heating have been tried but the most reliable and reproducible absorption mechanism has proven to be the electron Landau damping.

LH wave also exhibits a cut-off ($N_\perp \to 0$) when the nominator of Eq. (11) goes to zero. For the slow wave this can happen only when $C \to 0$ that is

$$C = P((N_\parallel - S)^2 - D^2) = 0 \tag{13}$$

The condition $(N_\parallel^2 - S)^2 = D^2$ produces the cut-offs of the fast wave

$$N_\parallel^{\mathrm{FC}} = \sqrt{S + D}, \tag{14}$$

and the condition $P = 0$ gives the LH-wave (slow-wave) cut-off. Again, in the limit $\omega_{ci} \ll \omega \ll \omega_{ce}$, the LH cut-off condition can be solved to give the cut-off density

$$n_c = \frac{\epsilon_0 m_e}{e^2} \omega^2 \propto \omega^2. \tag{15}$$

The cut-off density is an important parameter for the coupling because the wave can not propagate below it. Below the cut-off density the wave is evanescent and it can only tunnel into the higher densities. The LH wave is expected to reflect almost totally if the distance between the cut-off layer and the grill mouth is too large compared to the wavelength. Notice that we have 6-cm wavelength for KSTAR 5.0-GHz LHCD system.

When the lower hybrid resonance does not exist in the plasma, that is, $\omega > \omega_{LH}$, the condition for wave penetration to the maximum density without mode conversion to the fast wave is

$$N_{\parallel\, crit} = \frac{\omega_{pe}}{\omega_{ce}} + S^{1/2}. \tag{16}$$

This is well-known accessibility condition. Above equation is obtained with the approximation of S in Eq. (3) and iD in Eq. (4) in the limit of $\omega_{ci} \ll \omega \ll \omega_{ce}$. This critical value may be called linear turning point as shown in figures in next chapter.

8.3 Phase Velocity and Group Velocity

In the valid limit $N_{\parallel}^2 \gg 1$, the use of Eq. (12) gives a simplified equation of Eq. (11)

$$\frac{N_{\perp}^2}{N_{\parallel}^2} = \frac{m_i}{m_e} \cdot \frac{\omega_{LH}^2}{\omega^2 - \omega_{LH}^2}. \tag{17}$$

This equation states that a wave with a certain $N_{\parallel}$ has also a certain $N_{\perp}$. Eq. (17) can be solved for the wave frequency as a function of the wave number. And it gives the group velocity of the wave

$$v_{g\parallel} = \frac{\partial \omega}{\partial k_{\parallel}} = \frac{\omega}{k_{\parallel}} \frac{\omega^2 - \omega_{LH}^2}{\omega^2}, \tag{18}$$

$$v_{g\perp} = \frac{\partial \omega}{\partial k_{\perp}} = \frac{\omega}{k_{\perp}} \frac{\omega_{LH}^2 - \omega^2}{\omega^2}. \tag{19}$$

The wave frequency ω is usually larger than the lower hybrid resonance frequency ω_{LH} implying that the perpendicular phase velocity $v_{p\perp} = \omega/k_{\perp}$ is negative with respect to the group velocity since the perpendicular group velocity in Eq. (19) must be positive. The relation between the phase velocity and the group velocity gives the interesting phenomenon

$$\frac{v_{g\parallel}}{v_{g\perp}} = -\frac{k_{\perp}}{k_{\parallel}}. \tag{20}$$

This suggests the phase velocity and the group velocity are at right angles in the cold plasma approximation. Another interesting thing is that the higher plasma density results in the smaller angle of the propagation cones to the toroidal direction. Because the $N_{\parallel}$ is determined from the grill structure and $N_{\perp}$ is increased as the plasma density increases. One should note that the wave vector $\vec{k}$ and the propagation direction are at right angles.

8.4 Parametric study of the 5.0-GHz LH-wave propagation in the KSTAR tokamak

In this section, we calculate the parametric dependence of the wave propagations in the KSTAR tokamaks. The main equilibrium parameters are summarized in Table 1. In this table, R_0 is the major radius, a is the plasma minor radius, $A = R_0/a$ is the aspect ratio, κ is the ellipticity, δ is the triangularity, R^{gr} is defined as the grill position of the LH antenna, $q(a)$ is the safety factor at the edge. The q factor is defined as

$$q(r) = \frac{RB_{\phi}(r)}{2\pi} \int ds \frac{1}{R^2 B_{\theta}(r)}, \tag{21}$$

Let us now specialize the simple circular plasma model in toroidal geometry with local toroidal coordinates (r, θ, ϕ). r is the radius measured from the magnetic axis of the torus, θ is the poloidal angle, and ϕ is the toroidal angle rotated with respect to vertical coordinate. We neglect the ellipticity

Table 1: The main equilibrium parameters of the KSTAR tokamak

Parameter	Value
I_p (MA)	2.0
B_T (T)	3.5
n_{e0} (m^{-3})	1.0×10^{20}
T_{e0} (keV)	$10 \sim 20$
R_0 (m)	1.8
a (m)	0.5
A	3.6
κ	2.0
δ	0.8
$q(a)$	3 - 10
R^{gr} (m)	2.3

and the triangularity in subsequent calculations. The magnetic field in this circular plasma is given as below

$$B_r = 0 \tag{22}$$

$$B_\theta = \sqrt{B_R^2 + B_Z^2} = \frac{\mu_0 I_p}{2\pi r}(1 - (1 - (r/a)^2)^{q(a)}) \tag{23}$$

$$B_\phi = R_0 B_T/(R_0 + r\cos\theta) \tag{24}$$

$$B^2 = B_r^2 + B_\theta^2 + B_\phi^2. \tag{25}$$

Here, the pitch angle, p, between magnetic field lines and the toroidal direction will be needed in our analysis. The variation along the midplane of the pitch angle, $p = \arctan B_{pol}/B_\phi$, where $B_{pol} = \sqrt{B_r^2 + B_\theta^2}$, is plotted in Fig. (6) for the KSTAR. And, the electron temperature and the density profiles are modelled to be parabolic-like as below

$$n_e(r) = n_e(0)\left(1 - r^2/a^2\right)^\alpha \tag{26}$$

$$T_e(r) = T_e(0)\left(1 - r^2/a^2\right)^\beta \tag{27}$$

$$T_i(r) = T_i(0)\left(1 - r^2/a^2\right)^\beta. \tag{28}$$

For both α and β less than 1, we have broad density and temperature profiles. If they are higher than 1, we get more peaked squared parabola.

Since the plasma frequencies ω_{pe} and ω_{pi} are functions of the density and the cyclotron frequencies ω_{ce} and ω_{ci} are functions of the magnetic field, those frequencies are given as functions of the radial coordinate of the plasma. Therefore, we get the perpendicular refractive index $N_\perp$ and the

critical parallel refractive index $N_{\parallel crit}$ as a function of the radial coordinate of the plasma.

For the KSTAR tokamak with the central density $n_e(0) = 1 \times 10^{20}$ m^{-3} and the toroidal magnetic field at the plasma center $B_0 = 3.5$ T and the LH frequency of 5.0 GHz, the critical parallel refractive index is 2.27. Without approximation of S and iD, the $N_{\parallel crit}$ is solved from equating $B^2 - 4AC = 0$ and it becomes 2.18 for the same parameter as above. Fig. 7 shows $N_{\parallel crit}$ as a function of radial coordinate for central densities $n_e(0) = 0.2, 0.5, 1.0$ in unit of 10^{20} m^{-3} with the broad profile ($\alpha = 1$).

Figure 8 shows $N_\perp$ as a function of radial coordinate for various $N_\parallel$ with the central density $n_e(0) = 1 \times 10^{20}$ m^{-3}. Each $N_\parallel$ values in ascending corresponds to the phase differences, 60°, 90°, 120°, and 150° between adjacent waveguides of the grill. One may find that there exists evanescent zone due to low edge plasma density. In addition, we find that the wave with the launched $N_\parallel$ value less than $N_{\parallel crit}$ cannot penetrate into the center and the mode conversion from the slow wave to the fast wave. In this figure, the solid line corresponds to the slow wave and the dotted line to the fast wave. If the central density decreases, the wave can penetrate into the center because $N_{\parallel crit}$ decreases as the plasma density decreases (see Eq. (16)).

Fig. 9 shows $N_\perp$ for various central densities with $N_\parallel = 2.14$. But, there exists the longer evanescent zone for the lower central density.

In Figs. 8 and 9, $N_\parallel$ values are maintained with constant value as the wave propagates into the plasma. However, it actually varies downward or upward in the tokamak which has toroidal geometry. The wavelength must become shorter in regions of a smaller major radius in order to accommodate the same number of wave periods within a shorter toroidal circumference. The toroidal mode number $n_\phi^{\rm gr}$, imposed by the grill located at $R^{\rm gr}$, is related to the toroidal component, $N_\phi^{\rm gr}$, of the refractive index vector at the grill, through $N_\phi^{\rm gr} = cn_\phi^{\rm gr}/(\omega R^{\rm gr})$. The constancy of the mode number ($n_\phi = n_\phi^{\rm gr}$) then requires the toroidal refractive index, $N_\phi = cn_\phi/(\omega R)$, to be inversely proportional to the major radius, i.e.

$$N_\parallel = N_\phi = \frac{R^{\rm gr}}{R} N_\phi^{\rm gr}. \tag{29}$$

This is a most basic toroidal effect, and will be called a "wedge effect". Fig. 10 shows that $N_\parallel$ is gradually increased as the wave propagates into the plasma. The two lines of Fig. 11 show the re-plots of $N_\perp$ in the case of $N_\phi^{\rm gr} = 2.14$ in Fig. 8 with the wedge effect and without wedge effect, respectively. Interesting thing is that the wedge effect increases the $N_\parallel$ value so that the wave can penetrate into the center.

8.4.1 Spectral gap and $N_\parallel$ shifting

There is an aspect of wave damping mechanism that has not been fully understood. The lower-hybrid waves in the current drive regime are theoretically expected to damp through Landau damping by resonantly interacting with electrons that are moving at speeds near the wave phase speed parallel to the magnetic field. The spectrum of waves launched into a tokamak plasma by an antenna has, however, a phase speed often much greater than

the thermal speed of electrons, and there are few electrons that are resonant with the waves. This gap between the parallel phase speed of launched waves and electron thermal speed is commonly known as the 'spectral gap.' Upshifting of $N_\parallel$ can fill this gap, causing the waves to damp. Although a direct experimental confirmation of $N_\parallel$ upshifting is difficult, it has, nevertheless, become widely accepted as an explanation for how the lower-hybrid waves damp in spite of the spectral gap. The spectral gap can be large or small depending upon the wave phase speed and electron temperature. There exists upper and lower bounds of $N_\parallel$ shifting during the wave propagation in a tokamak plasma. The main reason of $N_\parallel$ shifting comes from the toroidal effect.

The wavenumbers conjugate to the spatial coordinates (r, θ, ϕ) are given as

$$\vec{k} = (k_r, m_\theta/r, n_\phi/R). \tag{30}$$

Where, the toroidal mode number n_ϕ is a constant of motion due to the toroidal symmetry. The toroidal effects comes from the variation in m_θ and magnetic shear. By definition, the parallel wavenumber $k_\parallel = \omega N_\parallel/c$ along to the magnetic field is

$$k_\parallel = \frac{\vec{k}\cdot\vec{B}}{|\vec{B}|}. \tag{31}$$

The magnetic field is given by Eqs. (22)-(24). The perpendicular wavenumber $k_\perp$ to the magnetic field is given by

$$k_\perp^2 = |\vec{k}|^2 - k_\parallel^2. \tag{32}$$

Using Eq. (30) and the magnetic field components gives

$$k_\parallel^2 = \frac{m_\theta B_\theta/r + n_\phi B_\phi/R}{B^2} \tag{33}$$

$$k_\perp = k_r^2 + \frac{m_\theta B_\phi/r - n_\phi B_\theta/R}{B^2}. \tag{34}$$

Substituting $m_\theta B_\theta/r$ from Eq. (33) into Eq. (34) we obtain an equation for $k_\parallel$

$$(k_\parallel\sqrt{1-\gamma^2} - k_\phi)^2 = \gamma^2(k_\perp^2 - k_r^2) \tag{35}$$

where $\gamma = B_\theta/B$. The perpendicular wave vector $\vec{k_\perp}$ is a function of $k_\parallel$ through the local dispersion relation. From Eq. (35), noting that $k_r^2 \geq 0$, we obtain the expression

$$(k_\parallel\sqrt{1-\gamma^2} - k_\phi)^2 \leq \gamma^2(k_\perp^2). \tag{36}$$

In the electrostatic limit ($k_\perp^2 = -(P/S)k_\parallel^2$) from Eq. (10), Eq. (36) breaks into the following two inequalities:

$$N_\parallel = \frac{k_\parallel c}{\omega} \leq \left(\frac{c}{\omega}\right)\frac{k_\phi}{\sqrt{1-\gamma^2} - \sqrt{-P/S}\gamma} = N_{\parallel,\,\mathrm{up}} \tag{37}$$

$$N_{\parallel} = \frac{k_{\parallel} c}{\omega} \geq \left(\frac{c}{\omega}\right) \frac{k_{\phi}}{\sqrt{1-\gamma^2} + \sqrt{-P/S\gamma}} = N_{\parallel,\,\mathrm{down}}. \tag{38}$$

The right-hand side in Eq. (37) corresponds to the extreme upshift, and the right-hand side in Eq. (38) corresponds to the extreme downshift. They varies as function of the pitch angle and the dielectric tensor elements, S and P. The solution of $k_{\parallel}$ becomes infinite when the denominator of Eqs. (37) and (38) vanishes. If the denominator of the upshifting becomes very small under some conditions, the upper bound increases rapidly.

The admissible range of $N_{\parallel}$ is defined by the lowest upper bound, the highest lower bound, the fast wave cutoff, and the mode conversion to the fast wave. The variation of the admissible range of $N_{\parallel}$ as a function of the position defines a 'wave domain' (WD).

Waves with a high $N_{\parallel}$ value will damp strongly through electron Landau damping. The condition that the wave phase speed be a certain multiple, λ, of the electron thermal speed, v_e, can be expressed as,

$$N_{\parallel}^{dmp} = \frac{c}{\lambda v_e} \approx \frac{5.33}{\sqrt{T_e}}. \quad \text{[in unit of keV]} \tag{39}$$

For the phase speed equal to the three times the thermal speed ($\lambda = 3$), the damping is strong. The damping is exponentially weaker at a higher phase speed.

For the KSTAR tokamak plasma, the $N_{\parallel}$ shifting is investigated in the following figures for various plasma conditions: the central density $n_e(0)$, the central temperature $T_e(0)$, the plasma current I_p, the safety factor q, and the $\alpha = 1$ or 2. Fig. 12 shows the fast wave cutoff (FC) by Eq. (14) and the upshift and downshift of $N_{\parallel}$ (Eqs. (37) and (38)) as a function of the radial position in the mid-plane for the central density. The solid line corresponds to $n_e(0) = 0.5 \times 10^{20}\,\mathrm{m}^{-3}$ and the dotted line to $n_e(0) = 1.0 \times 10^{20}\,\mathrm{m}^{-3}$. The other plasma parameters, $I_p = 2$MA, $q = 3$, $\alpha = 1$, and $N_{phi}^{\mathrm{gr}} = 2.14$. Note that this plot includes the wedge effect. From this figure, it is shown that the higher central density plasma gives more upshift in $N_{\parallel}$. The Landau damping zones are over plotted for various central electron temperature in Fig. 13. In this figure, the solid line in Fig. 12 is used for the $N_{\parallel}$ shifting. The damping zone (DZ) is defined as the overlap region between the wave domain region and the Landau damping region in Fig. 13. As the central electron temperature decreases, the damping zone goes to the upper region of the wave domain and hence the narrower region for the damping.

The $N_{\parallel}$ shifting is also investigated for the plasma current variations. With the plasma conditions of $n_e(0) = 1 \times 10^{20}\,\mathrm{m}^{-3}$, $\alpha = 1$, $q = 3$, and $N_{\phi}^{\mathrm{gr}} = 2.14$, the $N_{\parallel}$ shifting is plotted in Fig. 14. In this figure, the more upper shifting happens for the higher plasma current.

For $\alpha = 2$, we get a peaked profile of the electron density. We compared the $N_{\parallel}$ shifting of the broad profile with that of the peaked profile in Fig. 15. The figure shows that the broad profile gives more upshifting with few change of the downshifting. Here, we used $n_e(0) = 1 \times 10^{20}\,\mathrm{m}^{-3}$, $T_e(0) = 10$ keV, and $I_p = 2$ MA.

The dependency of the $N_{\parallel}$ shifting on the launched parallel refractive index N_{ϕ}^{gr} is shown in Fig. 16. When we get the higher launched value of N_{ϕ}^{gr} at the grill, the overall shifting is shifted up. In addition, the range

between the upper limit of the upshift and the lower limit of the downshift increases as shown in Fig. 17. The upper limits and the lower limits are also indicated inside the brace for each case of the launched N_{ϕ}^{gr} values. These values are obtained for $n_e(0) = 1 \times 10^{20}$ m^{-3}, $T_e(0) = 10$ keV, and $I_p = 2$ MA.

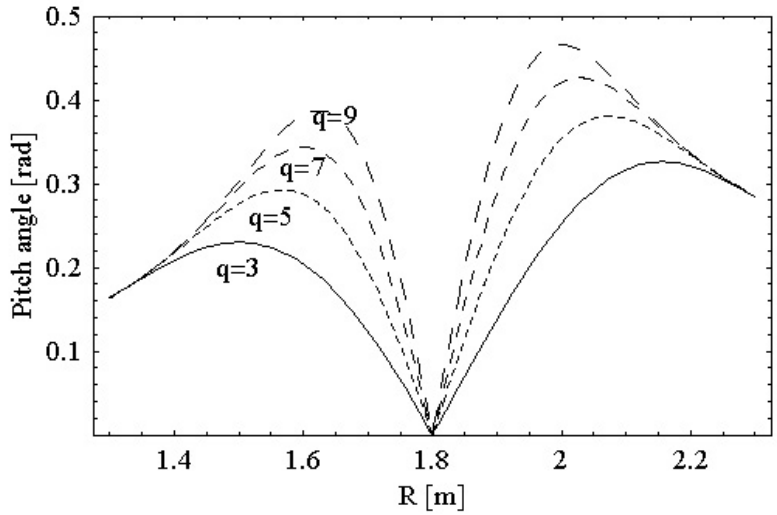

Figure 6: The magnetic pitch angle of KSTAR plasma in mid-plane. I_p = 2 MA and B_0 = 3.5 T

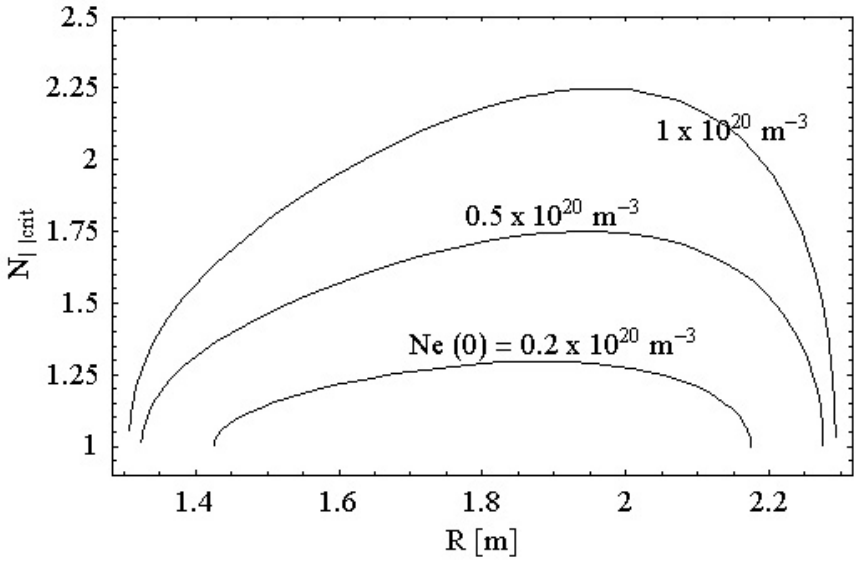

Figure 7: The critical $N_{\|}$ value vs radial position in mid-plane for various central density. Broad density profile ($\alpha = 1$) is used in this plot.

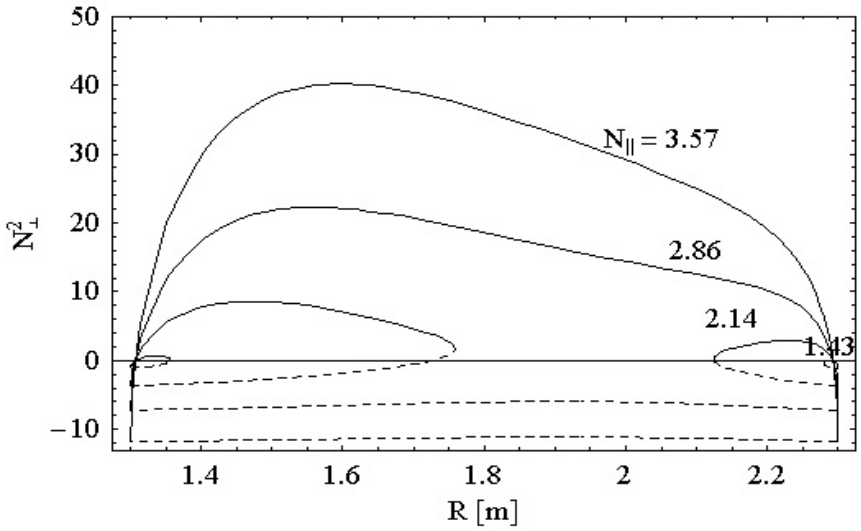

Figure 8: The perpendicular refractive index vs radial position in mid-plane for various $N_\phi^{\rm gr}$. $n_e(0) = 1.0 \times 10^{20}$ m^{-3} and $\alpha = 1$.

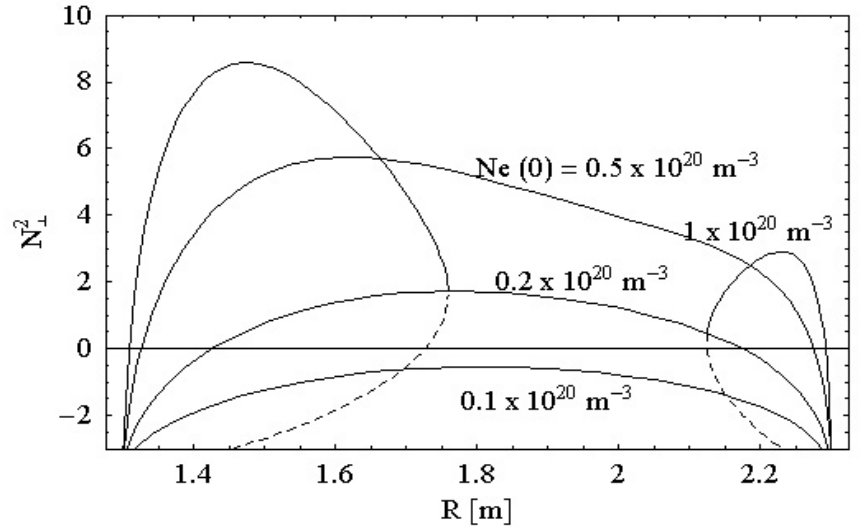

Figure 9: The perpendicular refractive index vs radial position in mid-plane for various central density. $N_\phi^{\rm gr} = 2.14$ and $\alpha = 1$.

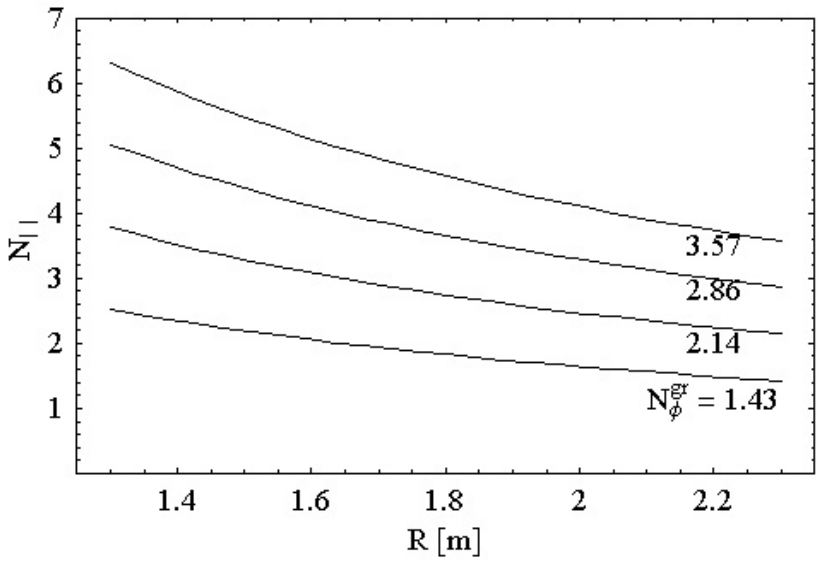

Figure 10: The variation of N_ϕ vs radial position.

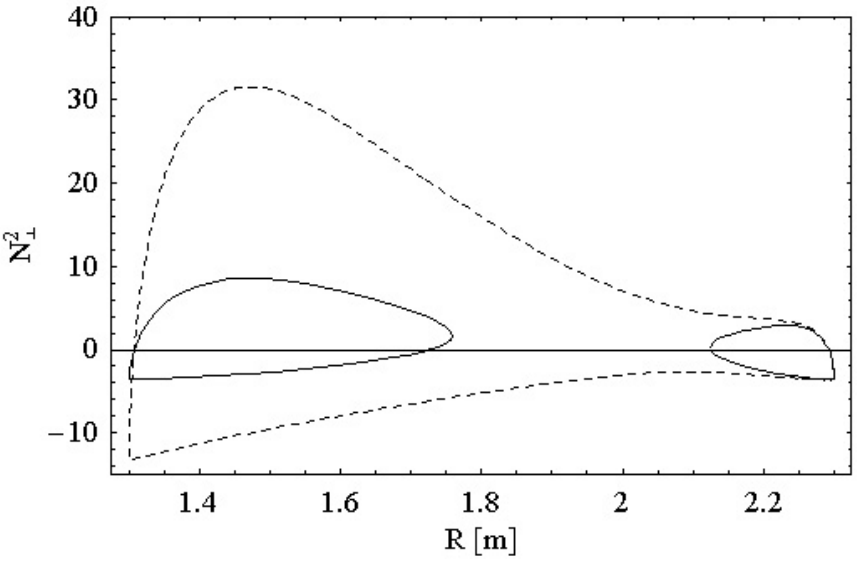

Figure 11: $N_\perp^2$ vs radial position in mid-plane with constant $N_\phi = N_\phi^{\rm gr} = 2.14$ (solid line) and with increasing N_ϕ due to wedge effect.

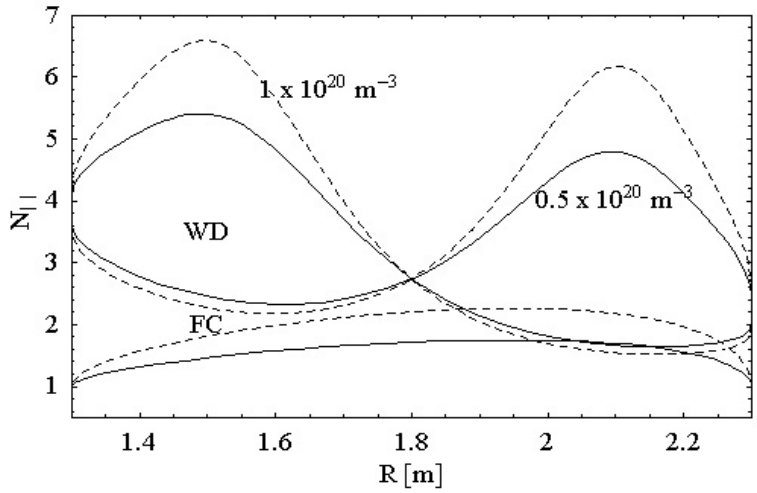

Figure 12: The up-shift and down-shift in $N_{\|}$ and the fast wave cut-off (FC) for two central densities and fixed $T_e(0) = 20$ keV. The "WD" is defined as the region bounded by up and down shifts and FC. Here, $N_\phi^{\rm gr} = 2.14$.

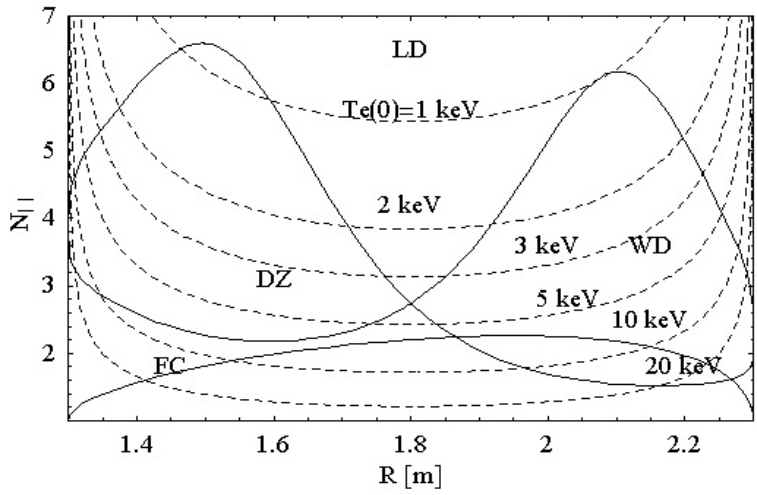

Figure 13: The wave domain and damping zone in KSTAR plasma for $n_e(0) = 1 \times 10^{20}$ m^{-3} with broad profile. The dashed lines are the significant Landau damping for various central temperatures. Here, $N_\phi^{\rm gr} = 2.14$.

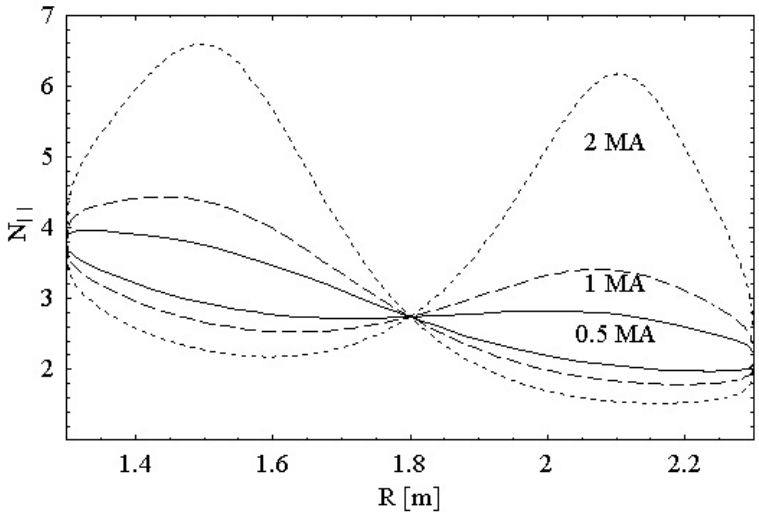

Figure 14: The up-shift and down-shift in $N_{\|}$ vs radial position in mid-plane for the plasma current. Here, $N_{\phi}^{\rm gr} = 2.14$.

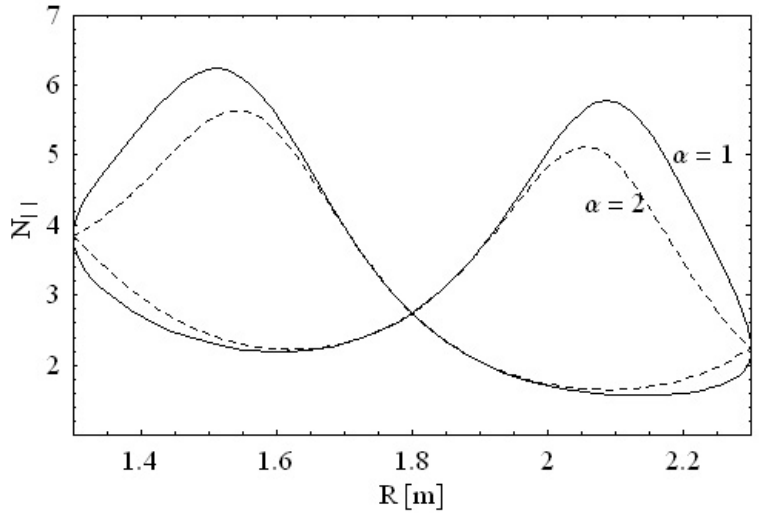

Figure 15: The up-shift and down-shift in $N_{\|}$ vs radial position in mid-plane for broad and peaked profiles. Here, $N_{\phi}^{\rm gr} = 2.14$.

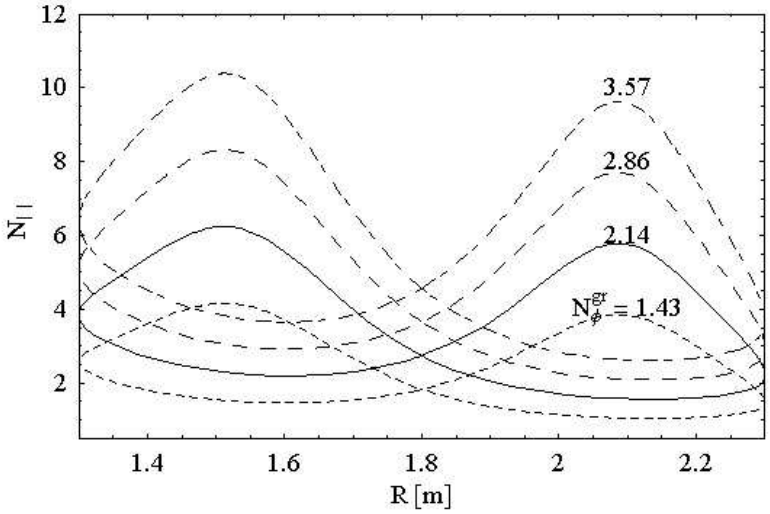

Figure 16: The up-shift and down-shift in $N_{\|}$ vs radial position in mid-plane for N_{ϕ}^{gr}.

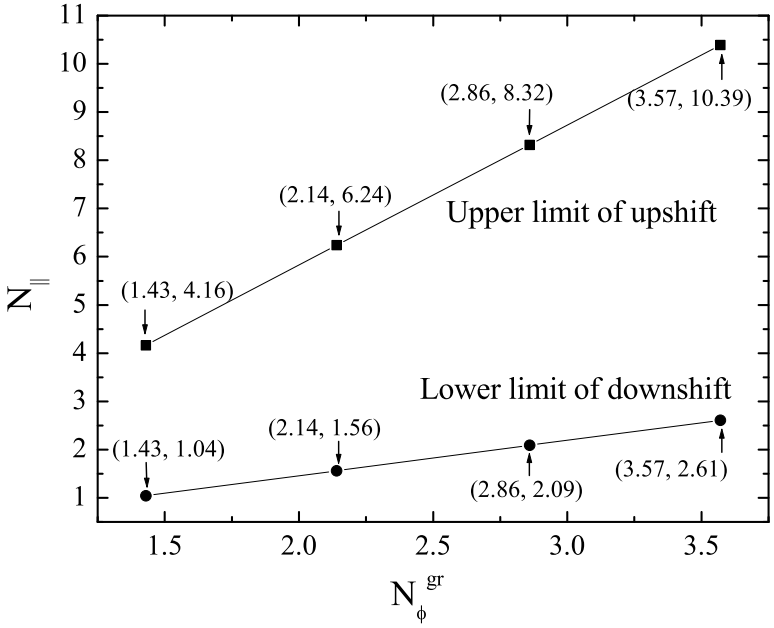

Figure 17: The upper limits of up-shift and the lower limits of down-shift vs N_{ϕ}^{gr}, which are results from Fig. 16.

8.5 Dispersion relation with thermal correction

The local dispersion relation can be written

$$D(\vec{r},\vec{k},\omega) = |\vec{k}\vec{k} - k^2 + (\omega^2/c^2)\overleftrightarrow{K}(\vec{r},\vec{k},\omega)| = 0 \tag{40}$$

if the electromagnetic portions of Maxwell's equations are retained or

$$D(\vec{r},\vec{k},\omega) = \vec{k}\cdot\overleftrightarrow{K}(\vec{r},\vec{k},\omega)\cdot\vec{k} = 0 \tag{41}$$

in the electrostatic approximation assuming $N_\parallel = k_\parallel c/\omega \gg 1$, hence therefore $\nabla\times\delta\vec{E} = \vec{k}\times\delta\vec{E} \simeq 0$. Here $\overleftrightarrow{K}$ is the hot plasm dielectric tensor (see section 3. Much of the physics of the propagation is found by a "warm-plasma" expansion of $\overleftrightarrow{K}(\vec{r},\vec{k},\omega)$ in which first-order temperature effects for ions and electrons are retained. After such an expansion (see section 3.1 and 3.2, Eq. (40) becomes

$$\begin{aligned} D(\vec{r},\vec{k},\omega) \;=\; & k_\perp^4 K_\perp \\ & + k_\perp^2\left([k_\parallel^2 - (\omega^2/c^2)K_\perp](K_\parallel + K_\perp) + (\omega^2/c^2)(K_{xy}^2 + 2K_{xy}K_2)\right) \\ & + K_\parallel\left([k_\parallel^2 - (\omega^2/c^2)K_\perp]^2 - (\omega^4/c^4)K_{xy}^2\right) = 0, \end{aligned} \tag{42}$$

and

$$D(\vec{r},\vec{k},\omega) = k_\perp^2 K_\perp + k_\parallel^2 K_\parallel = 0, \tag{43}$$

where

$$K_\perp = S - \alpha k_\perp^2;\;\; \alpha = 3\frac{\omega_{pi}^2}{\omega^2}\frac{V_{Ti}^2}{\omega^2} + \frac{3}{4}\frac{V_{Te}^2}{\omega_{ce}^2}, \tag{44}$$

$$K_\parallel = P\left(1 - \frac{k_\perp^2 V_{Te}^2}{\omega_{ce}^2} + 3\frac{k_\parallel V_{Te}^2}{\omega^2}\right), \tag{45}$$

$$K_{xy} = D\left(1 - \frac{3}{2}\frac{k_\perp^2 V_{Te}^2}{\omega_{ce}^2}\right), \tag{46}$$

$$K_2 = \frac{\omega_{pe}^2}{\omega\omega_{ce}}\frac{k_\parallel^2 V_{Te}^2}{\omega^2}, \tag{47}$$

$$V_{Ti,\,e}^2 = \frac{\kappa T_{i,\,e}}{m_{i,\,e}}. \tag{48}$$

The thermal corrections are also valid if $k_\perp^2 V_{Ti}^2/\omega^2$, $k_\perp^2 V_{Te}^2/\omega_{ce}^2$, $k_\parallel^2 V_{Te}^2/\omega^2$ are all much less than unity, and above equations can be rewritten

$$K_\perp = S - \alpha k_\perp^2;\;\; \alpha = 3\frac{\omega_{pi}^2}{\omega^2}\frac{V_{Ti}^2}{\omega^2} + \frac{3}{4}\frac{V_{Te}^2}{\omega_{ce}^2}, \tag{49}$$

$$K_\parallel = P, \tag{50}$$

$$K_{xy} = D, \tag{51}$$

$$K_2 = 0, \tag{52}$$

$$V_{Ti,\,e}^2 = \frac{\kappa T_{i,\,e}}{m_{i,\,e}}. \tag{53}$$

8.6 Wave absorption

An estimate of the wave absorption can be found only adding imaginary parts to the dispersion relation according to the imaginary parts of the plasma dispersion or Z function of Fried and Conte contained in the expressions for $\overleftrightarrow{K}(\vec{r},\vec{k},\omega)$. The asymptotic expansion of the Z function is useful for finding the good approximation of the damping term

$$\begin{aligned} Z(x) &= \frac{1}{\sqrt{\pi}}\int_{-\infty}^{\infty}\frac{\exp(-t^2)}{t-x}dt \\ &\simeq i\sqrt{\pi}\exp(-x^2) - (\frac{1}{x}+\frac{1}{2x^3}+\frac{3}{4x^5}+\ldots). \end{aligned} \tag{54}$$

It is important to note the appearance of the imaginary term in Eq. (55), arising from the pole contribution at $t = x$. This resonant part will give rise to a collisionless (or Laundau) damping of the Lower-hybrid wave. The damping terms for the electrons and ions (d_e, d_i) to be added to the electrostatic equation Eq. (43).

$$D = \Re(D) + i\Im(D) = D_r + iD_i = k_\perp^2 K_\perp + k_\parallel^2 K_\parallel + i(d_e + d_i) \tag{55}$$

The decrease in wave power P due to electron Landau damping and ion Landau damping is given by

$$P = P_0 \exp\left(-2\int \Im(k_\perp)dr\right). \tag{56}$$

The expansion of Eq. (55) about the real term of $k_\perp$ to the first order of the imaginary part of $k_\perp$ gives the expression of the $\Im(k_\perp)$.

$$\Im(k_\perp) = \frac{d_e + d_i}{(\partial D/\partial k_\perp)_{k_\perp = k_{\perp,r}}} = \frac{d_e + d_i}{[2k_\perp(\partial D/\partial k_\perp^2)]_{k_\perp = k_{\perp,r}}}. \tag{57}$$

With the help of good approximations of

$$\lambda_{e,i} = \frac{k_\perp^2 V_{Te,i}^2}{\omega_{ce,i}^2} \ll 1, \tag{58}$$

$$\chi_i = \frac{\omega}{\sqrt{2}k_\perp V_{Ti}} \gg 1, \tag{59}$$

$$\xi_e = \frac{\omega}{\sqrt{2}k_\parallel V_{Te}} \gg 1, \tag{60}$$

the damping terms d_e and d_i are expressed simply as

$$d_e = \frac{\sqrt{2}\omega_{pe}^2}{V_{Te}^2}\frac{\omega}{\sqrt{2}k_\parallel V_{Te}}\exp\left(-\frac{\omega^2}{2k_\parallel^2 V_{Te}^2}\right), \tag{61}$$

$$d_i = \frac{\sqrt{2}\omega_{pi}^2}{V_{Ti}^2}\frac{\omega}{\sqrt{2}k_\perp V_{Ti}}\exp\left(-\frac{\omega^2}{2k_\perp^2 V_{Ti}^2}\right). \tag{62}$$

One may note that $\lambda_{e,i}$ is the argument of the modified Bessel function and χ_i and ξ_e are the arguments of the Z function. With Eqs. (59)-(61), Eq. (57) are rewritten as

$$\frac{\Im(k_\perp)}{\Re(k_\perp)} = \frac{\sqrt{\pi}}{\partial D/\partial k_\perp^2}\left(F(\xi_e)\frac{\omega_{pe}^2}{\omega^2}\frac{k_\parallel^2}{k_\perp^2} + F(\chi_i)\frac{\omega_{pi}^2}{\omega^2}\right). \tag{63}$$

Where, the function $F(x) = x^3\exp(-x^2)$.